Remote Sensing of Environment 155 (2014) 303–311

Contents lists available at ScienceDirect

Remote Sensing of Environment

journal homepage: www.elsevier.com/locate/rse

Semi-empirical modeling of the scene reflectance of snow-covered boreal forest: Validation with airborne spectrometer and LIDAR observations

Jouni Pulliainen [a], Miia Salminen [a,b,*], Kirsikka Heinilä [b,c], Juval Cohen [a], Henna-Reetta Hannula [a]

[a] Finnish Meteorological Institute, P.O. Box 503, FI-00101 Helsinki, Finland
[b] Finnish Environment Institute, P.O. Box 140, FI-00251 Helsinki, Finland
[c] Department of Geosciences and Geography, University of Helsinki, P.O. Box 64, FI-00014 Helsinki, Finland

ARTICLE INFO

Article history:
Received 25 April 2014
Received in revised form 1 September 2014
Accepted 4 September 2014
Available online 20 September 2014

Keywords:
Snow reflectance
Remote sensing of snow
Boreal forests
Space-borne observed scene reflectance
Seasonal snow

ABSTRACT

This work aims at the development and validation of a zeroth order radiative transfer (RT) approach to describe the visible band (555 nm) reflectance of conifer-dominated boreal forest for the needs of remote sensing of snow. This is accomplished by applying airborne and mast-borne spectrometer data sets together with high-resolution information on forest canopy characteristics. In case of aerial spectrometer observations, tree characteristics determined from airborne LIDAR observations are applied to quantify the effect of forest canopy on scene reflectance. The results indicate that a simple RT model is feasible to describe extinction and reflectance properties of both homogeneous and heterogeneous forest scenes (corresponding to varying scales of satellite data footprints and varying structures of forest canopies). The obtained results also justify the application of apparent forest canopy transmissivity to describe the influence of forest to reflectance, as is done e.g. in the *SCAmod* method for the continental scale monitoring of fractional snow cover (FSC) from optical satellite data. Additionally, the feasibility of the zeroth order RT approach is compared with the use of linear mixing model of scene reflectance. Results suggest that the non-linear RT approach describes the scene reflectance of a snow-covered boreal forest more realistically than the linear mixing model (in case when shadows on tree crowns and surface are not modeled separately, which is a relevant suggestion when considering the use of models for large scale snow mapping applications).

1. Introduction

The appearance of seasonal snow cover and its melting dominate the annual hydrological and climatic patterns in vast regions of boreal forests and tundra in the Northern Hemisphere. Spatial and temporal changes in global snow cover are strongly connected to changes in Earth surface albedo and permafrost, and they, in turn, can have large effects on global carbon cycling, radiation balance and climate conditions (Barnett, Adam, & Lettenmaier, 2005; Betts & Ball, 1997; Brown & Mote, 2009). The Northern Hemisphere snow cover extent has decreased since the mid-1900, in particular in spring, due to climate change (Brown & Mote, 2009; Choi, Robinson, & Kang, 2010; Robinson, Dewey, & Heim, 1993; Vaughan et al., 2013). Long-term time series of satellite data estimates on seasonal snow cover extent (and its albedo) are needed for constructing climate data records (CDR) essential for climate research whereas near-real-time observations are needed for hydrological forecasting and water resource management; see e.g. Hall and Riggs (2007) and Vaughan et al. (2013). Currently, the available optical satellite data records for the Northern Hemisphere snow monitoring reach back for several decades; nearly 50 years (Robinson et al., 1993; Vaughan et al., 2013). Various algorithms for different sensors are summarized and evaluated by Dietz, Kuenzer, Gessner, and Dech (2012), Frei et al. (2012) and Nolin (2010). The usefulness of satellite data based results is strongly dependent on the quality of the interpretation (Hall & Riggs, 2007; Rittger, Painter, & Dozier, 2013). Imprecise remote sensing retrievals used as input may cause uncertainties to climate change predictions and hydrological modeling results (Rittger et al., 2013; Robinson et al., 1993; Vaughan et al., 2013). Despite the several feasible approaches to snow mapping there are defects that decrease their performance, e.g. the presence of cloud cover (Dietz, Wohner, & Kuenzer, 2012; Hall & Riggs, 2007). Lower accuracy in snow mapping is also typical in the transitional snowmelt areas and especially in the case of forested regions (Dietz, Kuenzer, et al., 2012; Hall & Riggs, 2007; Rittger et al., 2013). The effect of forest cover to the satellite observations applied to snow monitoring is the topic of this study.

The binary (two classes: snow-covered or snow-free) methods, such as the National Oceanic and Atmospheric Administration (NOAA)

* Corresponding author at: Finnish Meteorological Institute, P.O. Box 503, FI-00101 Helsinki, Finland. Tel.: +358 50 4485476.
E-mail address: miia.salminen@fmi.fi (M. Salminen).

http://dx.doi.org/10.1016/j.rse.2014.09.004

multisensor snow mapping method or the National Space Administration (NASA) Global Moderate Resolution Imaging Spectroradiometer (MODIS) snow map production, are mostly effective in large scale snow detection yielding products with good spatial and temporal resolution (Hall, Riggs, Salomonson, DiGirolamo, & Bayr, 2002; Helfrich, McNamara, Ramsay, Baldwin, & Kasheta, 2007; Ramsay, 1998). However, there are extensive areas in the northern latitudes with seasonal snow (annual accumulation and ablation of snow), where relatively large satellite data pixels are not fully snow covered or snow-free. Moreover, the satellite footprint often contains both forested and non-forested proportions in regions with seasonal snow causing wide-ranging problems in snow mapping when optical methods are used (Hall & Riggs, 2007; Hall, Foster, Salomonson, Klein, & Chien, 2001, Hall, Foster, Verbyla, Klein, & Benson, 1998; Klein & Barnett, 2003; Klein, Hall, & Riggs, 1998; Nolin, 2004; Parajka & Blöschl, 2006). Metsämäki et al. (2012) showed that MODIS baseline algorithm for FSC mapping (Salomonson & Appel, 2004, 2006) tends to strongly underestimate snow cover, in particular under dense canopy. The trees prevent visibility to snow covered or snow-free forest floor, whereas the crown layer and the related shadows contribute to the satellite observations. Apart from that, the proportion of (snow covered or snow-free) forest floor visible to the satellite sensor varies according to the sensor view zenith angle (Liu et al., 2008; Nolin, 2004). The inevitably erroneous binary mapping results for the boreal forest zone impair the further exploitation of the snow mapping retrievals; this includes the obtained often artificially narrow continental scale snowline instead of the actual wider transitional patchy snow zone.

Further approaches have been developed to obtain the fraction of snow covered area i.e. the fractional snow cover (FSC) within a pixel (Painter, Dozier, Roberts, Davis, & Green, 2003, Painter et al., 2009; Salomonson & Appel, 2004, 2006; Vikhamar & Sohlberg, 2002, Vikhamar & Solberg, 2003). Nonetheless, majority of the developed linear unmixing methods assume that the tree crowns are opaque (Painter et al., 2003, 2009; Vikhamar & Sohlberg, 2002, Vikhamar & Solberg, 2003). Several studies indicate that the other FSC retrieval algorithms also have problems in discerning snow beneath forest canopies (Metsämäki, Vepsäläinen, Pulliainen, & Sucksdorff, 2002; Nolin, 2010; Rittger et al., 2013; Salomonson & Appel, 2004). To compensate the adverse influence of the forest canopy to snow algorithm performance, these effects have to be reliably modeled. Often, snow mapping algorithms are founded on an inverse solution of a forward model that describes the satellite observation. The success of the method over forested regions is dependent on how well the model represents the forest canopy effect. So far, there are three methods for the forward modeling of forest effects in optical remote sensing of snow (Table 1). In the case of boreal forests, trees are apparently not opaque (see e.g. Painter et al., 2003, 2009 and Schlerf & Atzberger, 2006). Therefore, algorithms that treat forest canopy as a partially transparent layer have been developed and also implemented for operational use. An example of such approach is the *SCAmod* method for the mapping of FSC (Metsämäki, Anttila, Huttunen, & Vepsäläinen, 2005). *SCAmod* has been applied to a hemispheric scale in ESA DUE-GlobSnow (Luojus et al., 2010; Metsämäki et al., 2012). In *SCAmod*, forested areas are considered as a single forest canopy layer (permeable to light), characterized by a canopy transmissivity and reflectance according to the zeroth order radiative transfer theory. The apparent forest transmissivity in *SCAmod* is related to the fraction of forest floor visible from above and the penetration of light through the canopy. Basically, more advanced methods can be constructed by combining radiative transfer for considering trees and physical optics to account for openings between the trees (Li, Strahler, & Woodcock, 1995; Liu et al., 2008; Rosema, Verhoef, Noorbergen, & Borgesius, 1992; Schlerf & Atzberger, 2006). This kind of models can be called as hybrid models.

Table 1 summarizes the three basic modeling approaches for forest canopy effects to scene reflectance; geometrical optics (GO) with opaque trees, radiative transfer (RT) and hybrid modeling. Additionally, some typical empirical snow retrieval algorithms are listed in Table 1. These empirical algorithms are often based on the employment of NDSI (with thresholding) (Hall et al., 2002; Salomonson & Appel, 2004, 2006). Apart from using NDSI, NDVI (derived during summer) can be useful in snow algorithms to estimate vegetation density when the goal is the reduction of disturbances due to forests (Nolin, 2004). Alternatively, static maps of land cover or forest properties could be considered as input to snow algorithms but they suffer from infrequent updating. Hall et al. (1998), Klein et al. (1998) and Nolin (2004) suggested the estimation of forest properties by using satellite observations on fully snow covered forests. These can be considered preliminary to the *SCAmod* that has operationally applied this approach. The *SCAmod*

Table 1
Methods for the forward modeling of forest effects in optical remote sensing of snow and related snow parameter retrieval algorithms. Selected examples of empirical snow mapping methods applied to forested regions are also included.

Author	Forward (forest) model	Related (snow) inversion approach	Comments
	GO (geometrical optics)		GO considers tree canopy opaque
Li & Strahler (1985)[a]	(Linear) spectral mixing	–	Forest stand model
Painter et al. (2003, 2009)	-II-	(Linear) spectral unmixing	MEMSCAG, MODSCAG (RT)[b] for FSC
Dozier, Green, Nolin, & Painter (2009)	-II-	(Linear) spectral unmixing	FSC, Albedo
Vikhamar and Sohlberg (2002), Vikhamar and Solberg (2003)	-II-	(Linear) spectral unmixing	*SnowFor* for snow-covered forest, *SnowFrac* for FSC
Salminen et al. (2009)	-II-	–	No shadowed/sunlit canopy components considered
	GO + RT (hybrid)		Hybrid considers tree canopy non-opaque, otherwise as GO
Schlerf and Atzberger (2006)	INFORM	–	More sophisticated/complex to FLIM
Rosema et al. (1992)	FLIM	–	Simplified model similar to INFORM
Niemi et al. (2012)	–	–	Simplified model similar to FLIM and INFORM
Li et al. (1995)	GORT	–	Spectral mixing forward model[c]
Liu et al. (2008)	GORT	–	Viewable (forest) Gap Fraction (VGF) estimated[d]
	RT radiative transfer		RT considers tree canopy non-opaque (turbid medium)
Metsämäki et al. (2005, 2012)	Zeroth order RT	Analytical inverse solution	*SCAmod* for FSC
Klein et al. (1998)	GeoSAIL	–	Thresholds for MODIS binary algorithm
Salomonson and Appel (2004, 2006)	–	Empirical	Linear regression algorithm (using NDSI) for FSC[e]
Hall et al. (2002)	–	-II-	Snow binary classification using NDSI and NDVI[f]

[a] Later spectral mixing models are based on Li and Strahler (1985) that consider shadows and directly illuminated background.
[b] Reflectance of the opaque tree canopy can be calculated for MODSCAG using the RT model (Liu et al., 2008; Painter et al., 2009).
[c] For partially non-opaque forest canopy.
[d] Airborne LIDAR data-aided model parameterization.
[e] MODIS fractional method.
[f] MODIS binary method based on Klein et al. (1998).

algorithm is an example of an approach that attempts to compensate for the effects of forest cover based on the use of the zeroth order RT approach for the forward modeling of the influence of forest canopy (Metsämäki et al., 2005, 2012). In practice, this is carried out with the aid of forest canopy transmissivity estimated from the optical satellite data that represents full snow cover conditions. More complicated hybrid forward modeling approaches have been also investigated in case of boreal forests, e.g. by applying mast-borne spectrometer observations where shadowing effects and gaps between trees have been considered (Niemi et al., 2012). This Niemi et al. (2012) model can be considered as a simplification of the approach used by Schlerf and Atzberger (2006). However, hybrid approaches are complicated and thereby difficult to apply to the satellite data inversion. Thus, the topic of this paper is concerned whether a simple zeroth order RT approach – that considers forests of a satellite pixel as a single layer of turbid medium – is valid for boreal forests and whether this approach applies to different scales. This is also a central issue concerning the basis of the *SCAmod* algorithm.

Earlier investigations of forest canopy effects in boreal forest zone have indicated that the assumption of opaque canopy does not hold, as discussed above. This is also apparent from the earlier work with data from the Sodankylä site (the experimental region of this investigation), as the hybrid approach in Niemi et al. (2012) indicated better agreement with observations than the (simplified) GO approach (Salminen, Pulliainen, Metsämäki, Kontu, & Suokanerva, 2009). Thus, the hybrid approaches are arguably physically most accurate for boreal forests. However, physical approaches are difficult for inversion purposes due to the model complexity. Therefore, a simpler RT approach is thoroughly investigated and validated here. This is accomplished by quantifying the effect of forest canopy on scene reflectance using tree characteristics determined from airborne LIDAR observations of high spatial accuracy. These data are compared with the predictions by the zeroth order RT modeling. The investigations are carried out at the condition of full thick snow cover on ground and with snow free canopy, which enables the separation of the effect of trees from that of soil/understory vegetation. The RT model performance is further compared with simplified linear GO approach (analogous to Li & Strahler, 1985), in order to find out whether the RT approach with a single forest canopy layer (in a footprint) explains the observations better than the simplified GO approach. The investigated and compared forward modeling approaches are such that they are feasible for the continental scale satellite data inversion, i.e. to be used for snow cover monitoring if detailed information on tree distribution are not available for a pixel scale (instead only bulk characteristics such as mean tree height, stem volume, canopy cover or apparent forest canopy transmissivity were available).

The investigation is carried out in Sodankylä region, northern Finland, which is a typical example of a classical boreal forest site. The airborne imaging and mast-borne forest plot monitoring spectrometer data sets provide unique material to investigate (a) the spatial behavior of scene reflectance at boreal forests and (b) the temporal variability of forest scene reflectance due to varying illumination geometries. The results shown here focus on the wavelength channel of 555 nm as this region is essential for the remote sensing of snow, and since earlier investigations for the Sodankylä site (Heinilä et al., 2014) demonstrated the results for other wavelength regions. The investigation is also restricted to the case of near-nadir observations due to the applied experimental data sets.

2. Materials

2.1. Test area, land cover and forest information

The test area in Sodankylä, northern Finland, represents a typical conifer-dominated northern boreal forest. The dominant species in the Sodankylä region are Scots pine and Norway spruce. Pine-dominated forests comprise 92% of the total forest area of the southern part of Finnish Lapland (METLA, 2010). Birches including dwarf birches are typical at wetlands. Fig. 1 shows the scenery of typical pine forests of the area. The detailed forest canopy characteristics corresponding to the airborne reflectance data acquisition are summarized in Table 2. In addition to the region of airborne surveys, the multi-temporal mast-borne spectrometer experiments were carried out for a single forest plot coinciding one of the flight lines. This particular plot represents pine forest on mineral soil with a canopy cover $C = 40\%$. Fig. 2 shows the land cover map of the study area with flight lines of airborne spectrometer observations (see also Fig. 4 in Heinilä et al. (2014)).

The forests of the Sodankylä test area are also inventoried using Airborne Laser Scanning (ALS), i.e. LIDAR observations. Tree characteristics determined from these data were applied as main reference data on forest properties of the site. The ALS data, with a point density of at least one point per 2 m^2, were provided by the National Land Survey (NLS) of Finland. These observations were used to create canopy cover percentage (C) and tree height (H) maps for a spatial ground resolution of 10 m. The first step in processing the LIDAR data was to create vegetation height (H) grids with a pixel size of 1 m for the C retrieval and 2 m for the H retrieval. The vegetation height grids were generated first by subtracting the ground level height (Digital Terrain Model) from the top of the vegetation height (Digital Surface Model) and then, by converting the resulted point cloud to grids of 1 m and 2 m pixel size. The second step was to generate the C map from the 1 m H grid and the H map from the 2 m H grid. The C was generated first by classifying 1 m by 1 m-sized pixels to either tree or no tree based on the height (the limit being 1.5 m) derived to ALS observation of that pixel. Then, the ratio between tree pixels and all pixels inside a grid cell of 10×10 m was calculated. The H map was generated by 1) removing low vegetation and water; 2) applying a circle shaped dilation (maximum) filter with a radius of 2 pixels (equivalent to 4 m on the ground) and; 3) calculating the mean height inside a grid cell of 10×10 m. The quality control for the retrieved maps was performed (at the spatial resolution of 20 m) by evaluating the retrieved maps against corresponding National Forest Inventory (NFI) digital maps (Tomppo, Haakana, Katila, & Peräsaari, 2008). For example, the correlation coefficient between NFI- and ALS-based C was found to be $r = 0.72$, RMSE $= 11.8\%$-units and BIAS $= 0.89\%$-units.

2.2. AISA airborne imaging spectrometer data

The employed airborne spectrometer data set was acquired on March 18, 2010 at cloud-free conditions; see Heinilä et al. (2014) for details. Trees were snow free during the airborne campaign, and the snow pack was dry (temperature −6 °C on average) and the air temperature was −4 °C at 10 UTC. Further, as described in Heinilä et al. (2014), the AISA imaging spectrometer data were radiometrically and

Fig. 1. Scots pine-dominated northern boreal forests at the Sodankylä site.

Table 2
Tree canopy characteristics of the Sodankylä test area at spatial scales of 10 m and 100 m (mineral soil and peat lands).

Forest characteristic	Mean	Median	Min/Max	Standard deviation
Canopy cover, C (%)				
10 m	24.4	22.5	0/100	20.3
100 m	24.7	24.9	0/59	15.1
Stem volume, V (m^3/ha)				
10 m	33.7	28.0	0/179	31.1
100 m	33.4	31.7	0/113	24.1
Tree height, H (m)				
10 m	7.5	7.3	0/24.2	5.1
100 m	7.1	7.2	0/17.8	4.3

geometrically corrected and mean-filtered to pixel size of 10 m. This investigation is performed using this 10 m gridded data together with ALS-based forest parameter data processed to the same grid. Fig. 3 depicts an example of the gridded airborne AISA spectrometer data at the channel of 545–565 nm used for analyses here (corresponding to MODIS band 4).

Since the field of View (FOV) of AISA observations is 17°, the analyses here are limited to near-nadir angles of observation (from 0° to 8.5° off nadir). As indicated in Fig. 2, the flight lines have varying orientations. Additionally, they were measured during an interval of one hour. Thus, the Sun zenith angle is close to 70° for all observations and the azimuthal angle difference between the direction of illumination and measurements has a relatively high range from 45° to 135°. As a consequence, both backscattering and forward scattering geometries are included in the airborne spectrometer data set.

2.3. Mast-borne and field spectrometry

The applied data sets include mast-borne ASD spectrometer observations from the day of airborne data acquisition (March 18, 2010), accompanied with observations from 12 days during the spring–winter of 2013 (also representing full snow cover conditions). All observations represent the same forest plot with the same sensor azimuth and look angle characteristics (measurement angle 11° off nadir); see Niemi et al. (2012) and Salminen et al. (2009) for details. These data are used for the analysis of the variability of forest scene reflectance due to varying illumination and viewing conditions. Since several mast-borne measurements were conducted for each day of observation, the data set includes both forward and backscattering geometries (corresponding to airborne data set). The Sun zenith angle varies from 59.0° to 77.2°, and the Sun azimuth and sensor view angle difference is from 2.7° to 136.5°. All data represents dry snow conditions with thick snow pack (tree canopy snow free).

In addition to mast-borne observations, nadir view-angle field spectrometry measurement of natural snow packs using a similar spectrometer system was applied to incorporate information on average level of dry snow reflectance (Salminen et al., 2009).

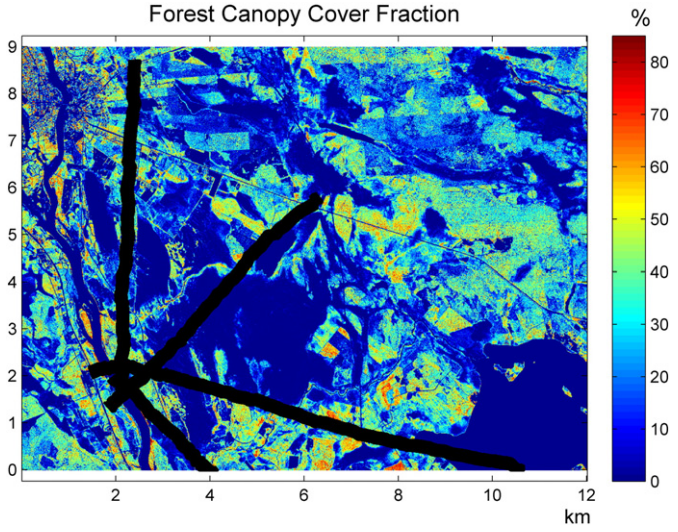

Fig. 2. AISA data from 18 March 2010 comprise four flight lines (depicted in black color). The underlying forest canopy cover (*C*) fraction is derived using LIDAR data.

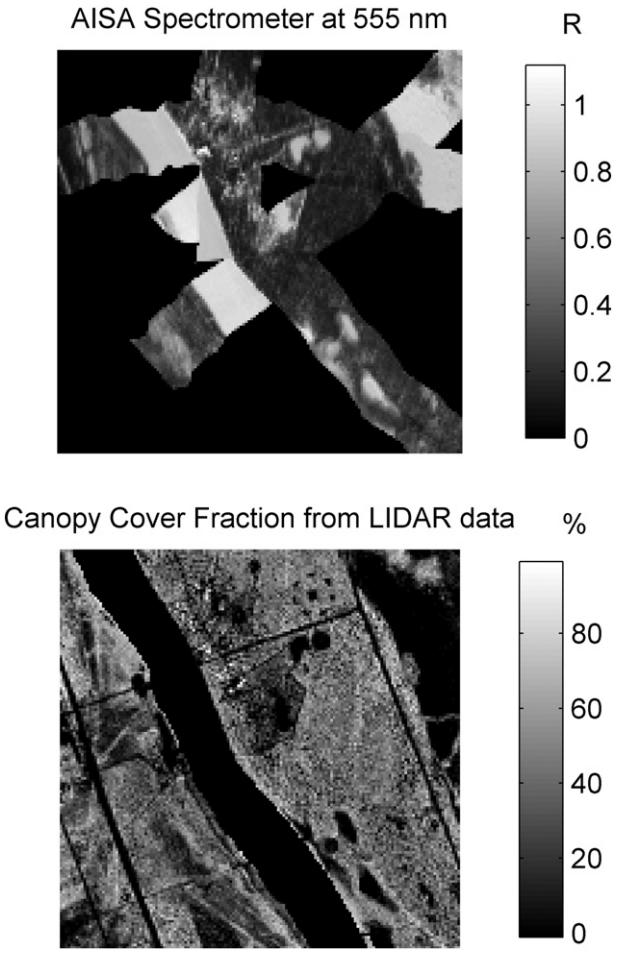

Fig. 3. A close-up of 18 March 2010 AISA data (above) and the corresponding canopy cover fraction obtained by using LIDAR data.

3. Methods

The scene reflectance of a (partially) snow-covered boreal forest at the wavelength λ can be modeled by an approach incorporating the reflectance contributions of snow-covered ground $\rho_{\lambda,snow}$ and snow-free ground $\rho_{\lambda,ground}$, and by considering the forest canopy as a partially transparent reflecting layer. When the model is based on the zeroth order solution of the radiative transfer equation (RT), the parameters that define the effects of the tree layer are the reflectance of an opaque forest canopy $\rho_{\lambda,forest}$ and the two-way forest canopy transmissivity t^2 (Metsämäki et al., 2005, 2012; Pulliainen, Heiska, Hyyppä, & Hallikainen, 1994; Salminen et al., 2009). Additionally, analogous approaches for the canopy transmissivity, or transmittance, with a different notation have been used e.g. by Schlerf and Atzberger (2006). Based on this approach, if the fraction of the terrain covered by snow

is denoted by *FSC* (ranging from 0 to 1), the model for the observed reflectance R_{mod} at the wavelength λ is obtained by

$$R_{\lambda,mod}(FSC) = \left(1-t_\lambda^2\right)\rho_{\lambda,forest} + t_\lambda^2\left[FSC\,\rho_{\lambda,snow} + (1-FSC)\,\rho_{\lambda,ground}\right]. \quad (1)$$

If the scene has a full snow cover on ground $FSC = 1$, we get

$$R_{\lambda,mod} = \left(1-t_\lambda^2\right)\rho_{\lambda,forest} + t_\lambda^2\,\rho_{\lambda,snow}. \quad (2)$$

The two-way forest canopy transmissivity t^2 in Eqs. (1) and (2) is related to the extinction properties of the vegetation canopy, which is discussed next.

3.1. Modeling of boreal forest scene reflectance based on the zeroth order solution of the radiative transfer (RT) equation

The zeroth order solution to RT equation excludes multiple scattering. Thus, analogous to Pulliainen et al. (1994), an analytical formula can be written to consider the effect of forest canopy to the reflected radiance (now on, ignoring λ for simplicity):

$$\frac{L(\theta_s)}{E_0(\theta_i)}\pi = \int_0^H \left[\pi\gamma_s(\theta_i,\theta_s,h)\exp\left(\int_0^{H-h}\frac{-\kappa_e(\theta_i,\theta_s,h')}{\cos(\theta_i)}dh'\right)\exp\left(\int_0^{H-h}\frac{-\kappa_e(\theta_i,\theta_s,h')}{\cos(\theta_s)}dh'\right)\right]dh \quad (3)$$

where L is the reflected radiance [W sr^{-1} m^{-2}], E_0 is the incoming irradiance above the canopy [W m^{-2}], $\pi\gamma_s$ is the reflectance of an infinitesimal volume unit and κ_e is the canopy extinction coefficient [1/m]. The concept of Eq. (3) illustrated in Fig. 4 shows the geometrical consideration of the approach: H is the total height of the forest canopy, h is the height within the canopy, θ_s is the angle of observation (scattering/reflection angle) and θ_i is the angle of incident radiation. According to Eq. (3) the total two-way transmissivity of the forest canopy along the directional path of light propagation is

$$t^2(\theta_i,\theta_s) = \exp\left(\int_0^H\frac{-\kappa_e(\theta_i,\theta_s,h)}{\cos(\theta_i)}dh\right)\exp\left(\int_0^H\frac{-\kappa_e(\theta_i,\theta_s,h)}{\cos(\theta_s)}dh\right). \quad (4)$$

If κ_e and $\pi\gamma_s$ are assumed to be constants as function of illumination and reflection angles and the height h within the forest canopy (Eq. 3) is simplified to

$$\frac{L(\theta_s)}{E_0(\theta_i)}\pi = \frac{\pi\gamma_s}{\kappa_e\left(\cos^{-1}(\theta_i)+\cos^{-1}(\theta_s)\right)}\left[1-t^2(\theta_i,\theta_s)\right] = \rho_{forest}\left[1-t^2(\theta_i,\theta_s)\right], \quad (5)$$

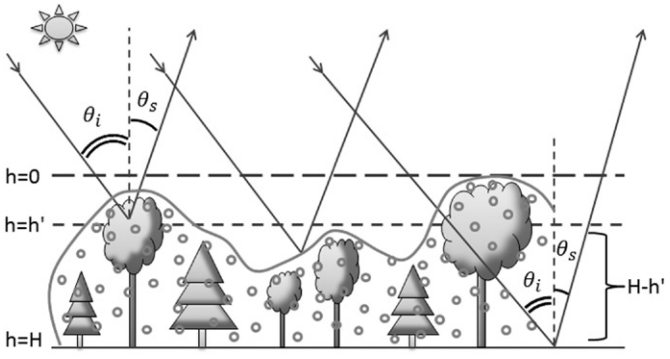

Fig. 4. Geometrical consideration of the bidirectional reflectance of a forest scene. θ_i is the incidence angle of incoming irradiance and θ_s is the angle of observation (and hence also the scattering angle under investigation in the forest canopy). The applied RT approach considers a forested scene (pixel) as a single turbid medium layer characterized by bulk volume scattering and extinction properties $\pi\gamma_s$ and κ_e; see Eq. (3).

thus, Eq. (5) provides the first term of Eq. (1), and the second term of Eq. (1) is simply the reflection from the snow-covered ground attenuated by the two-way forest canopy transmissivity. In the case of the two-way transmissivity t^2 the assumption of a constant extinction coefficient leads from Eq. (4) to:

$$t^2(\theta_i,\theta_s) = \exp\left(-\kappa_e H\left(\frac{1}{\cos(\theta_i)}+\frac{1}{\cos(\theta_s)}\right)\right). \quad (6)$$

To summarize, if scene reflectance is modeled for observation angles close to nadir $\theta_s \approx 0$, then $\cos^{-1}(\theta_i)+\cos^{-1}(\theta_s) \approx \cos^{-1}(\theta_i)+1$. Then by denoting $\cos^{-1}(\theta_i)+1 = 2g'(\theta_i)$, Eq. (2) can be rewritten as

$$R_{mod} = \left(1-\exp\left(-2\kappa_e g'(\theta_i)H\right)\right)\rho_{forest} + \exp\left(-2\kappa_e g'(\theta_i)H\right)\rho_{snow}. \quad (7)$$

3.2. Parametrization and validation of the model using airborne spectrometer and LIDAR data

In Eq. (7), the semi-empirical scene reflectance model, derived from the zeroth order solution of RT equation, is parameterized as a function of tree height H [m]. The model can be as well given as a function of canopy cover (C in %-units) or forest stem volume (V in m^3/ha) which is related to the product $V \sim C \times H$ (Heinilä et al., 2014). As discussed in Section 2.2 all canopy characteristics are derived from LIDAR observations. In the case of V, the product $C \times H$ is calibrated to volume estimate using a regression between the LIDAR data-derived product and NFI forest stem volume map (available with a coarser spatial resolution of 20 m).

Thus, we can write by denoting $\kappa_e = \kappa_{e,H}$, $\kappa_e = \kappa_{e,C}$ or $\kappa_e = \kappa_{e,V}$ when the formula is derived for tree height (H), canopy cover (C) or stem volume (V), respectively:

$$R_{mod,H} = \left(1-\exp\left(-2\kappa_{e,H}g'(\theta_i)H\right)\right)\rho_{forest} + \exp\left(-2\kappa_{e,H}g'(\theta_i)H\right)\rho_{snow} \quad (8a)$$

$$R_{mod,C} = \left(1-\exp\left(-2\kappa_{e,C}g'(\theta_i)C\right)\right)\rho_{forest} + \exp\left(-2\kappa_{e,C}g'(\theta_i)C\right)\rho_{snow} \quad 8b$$

$$R_{mod,V} = \left(1-\exp\left(-2\kappa_{e,V}g'(\theta_i)V\right)\right)\rho_{forest} + \exp\left(-2\kappa_{e,V}g'(\theta_i)V\right)\rho_{snow}. \quad 8c$$

Parameters κ_e, ρ_{snow} and ρ_{forest} in Eqs. (8a)–(8c) can be estimated for certain conditions by fitting the model into an observation data set representing certain specific measurement conditions. Here, the observational data consist of AISA measurements carried out at the Sodankylä site (see Section 2.3). Thus, the assumption is that the three parameters can be treated with their mean effective values over the image scene. The model fitting is performed by the least squares method by searching the global minimum for the cost function J with respect to κ_e, ρ_{snow} and ρ_{forest}:

$$J\left(\kappa_e,\rho_{forest},\rho_{snow}\right) = \sum_{i=1}^{N}\left(\left(R_{mod,i}(\kappa_e,\rho_{forest},\rho_{snow},\begin{Bmatrix}H_i\\C_i\\V_i\end{Bmatrix}\right) - R_{obs,i}\right)^2 \quad (9)$$

where sub-index i refers to an observation case with specific forest characteristics H_i, C_i and V_i. The fitting is carried out separately for H, C and V. That is, models by Eqs. (8a), (8b) and (8c) are fitted separately to observational data by estimating three scalars for each case.

As an outcome of the fitting procedure, the modeled response of scene reflectance to the two forest canopy (κ_e, ρ_{forest}) and one surface characteristic (ρ_{snow}) is obtained. As shown by Eqs. (8a)–(8c) this response is exponential. In order to assess the validity of the model fit, it is compared with the statistical performances of a linear fit (two parameters in fitting) and of a second-degree polynomial fit (three parameters

in the fitting as in the case of Eq. (9)). In practice, the correlation coefficient between the model prediction of reflectance and observed reflectance is determined for different approaches.

Especially, the comparison of the applied radiative transfer approach with linear modeling is essential, as the linear approach can be considered as a simpler characterization of the physical problem. In that case we can consider that the reflectance is an areally weighted sum of reflectance contributions from an opaque forest canopy and from surface, i.e. from openings between the trees:

$$\begin{aligned} R_{mod} &= C\rho_{forest} + (1-C)\rho_{snow} \\ &= C\left(\rho_{forest}-\rho_{snow}\right) + \rho_{snow} \\ &= a_1 C + a_0. \end{aligned} \quad (10)$$

Note that Eq. (10) is actually a simplification of the geometric optics approach introduced by Li and Strahler (1985). Thus, the comparison of Eqs. (8a)–(8c) and Eq. (10) with the experimental Sodankylä data enables the analysis whether the radiative transfer approach (Eq. 8) or geometric optics (Eq. 10) applies better to describe the reflectance observations as a function of quantitative forest canopy characteristics.

3.3. Assessment of spatial and viewing/illumination geometry related characteristics of boreal forest scene reflectance

The applied airborne imaging spectrometer and LIDAR data set also enables the investigation the effect of spatial scale to the modeling of observations. Due to image swath and LIDAR data processing limitations the influence of scale is here investigated from 10 m to 100 m. That is, the model parameters are estimated separately for data processed to the grid sizes ranging from 10×10 m^2 to 100×100 m^2. This is relevant to the point of view of satellite data retrieval approaches. For example *SCAmod* applies reflectance modeling in the scale of the employed satellite data (Metsämäki et al., 2012).

As described in Section 3.2, the analysis of aerial spectrometer data facilitates the determination of the spatial variability of scene reflectance as a function of forest canopy characteristics. Another important issue is the temporal variability of forest canopy reflectance, which is, ignoring bio-physical issues, sensitive to imaging geometry (Sun and instrument view angles). Since the mast-borne spectrometer data from a forest plot (described in Section 2.4) represents variable bidirectional measurement configurations, these data can be used to derive information on the temporal variability of forest canopy effects to observed scene reflectance. The basis of this consideration is the error propagation analysis of scene reflectance. We can write for the total variance of observed reflectance as a sum of contributions due to canopy extinction, snow reflectance and reflectance of an opaque forest canopy:

$$\mathrm{var}(R) = \mathrm{var}(R)_{|\kappa_e} + \mathrm{var}(R)_{|\rho_{snow}} + \mathrm{var}(R)_{|\rho_{forest}}. \quad (11)$$

When the variance contribution resulting from the temporal variability of forest canopy extinction coefficient ($\mathrm{var}(R)_{|\kappa_e}$ in Eq. (11)) is approximated through the Taylor-series expansion of Eq. (8b) we can rewrite Eq. (11) as

$$\begin{aligned} \mathrm{var}(R) &\approx \left(\frac{\partial R}{\partial \kappa_e}\right)^2 \mathrm{var}(\kappa_e) + \left(\frac{\partial R}{\partial \rho_{snow}}\right)^2 \mathrm{var}(\rho_{snow}) + \left(\frac{\partial R}{\partial \rho_{forest}}\right)^2 \mathrm{var}\left(\rho_{forest}\right) \quad (12) \\ &= \left[2g'C\left(\rho_{forest}-\rho_{snow}\right)\exp(-2\kappa_e g'C)\right]^2 \mathrm{var}(\kappa_e) \\ &\quad + \left[\exp(-2\kappa_e g'C)\right]^2 \mathrm{var}(\rho_{snow}) \\ &\quad + \left[1-\exp(-2\kappa_e g'C)\right]^2 \mathrm{var}\left(\rho_{forest}\right). \end{aligned}$$

Thus, the estimate on $\mathrm{var}(\kappa_e)$, the variance of forest canopy extinction coefficient, can be obtained by

$$\mathrm{var}(\kappa_e) = \frac{\mathrm{var}(R) - \left[\exp(-2\kappa_e g'C)\right]^2 \mathrm{var}(\rho_{snow}) - \left[1-\exp(-2\kappa_e g'C)\right]^2 \mathrm{var}\left(\rho_{forest}\right)}{\left[2g'C\left(\rho_{forest}-\rho_{snow}\right)\exp(-2\kappa_e g'C)\right]^2} \quad (13)$$

where the $\mathrm{var}(R)$ is directly determined from the multi-temporal observations of forested terrain reflectance of the single forest plot; see Niemi et al. (2012) and Heinilä et al. (2014). Note that the term $\exp(-2\kappa_e g'C)$ can be derived from the AISA data analysis of this investigation, whereas the terms ρ_{forest}, $\mathrm{var}(\rho_{forest})$, ρ_{snow} and $\mathrm{var}(\rho_{snow})$ can be derived from the results of earlier investigations (Niemi et al., 2012; Salminen et al., 2009).

When Eq. (13) is used to estimate the variance of the two-way forest canopy transmissivity, we can write:

$$\mathrm{var}\left(t^2\right) \approx \left[-2Cg' \exp(-2\kappa_e g'C)\right]^2 \mathrm{var}(\kappa_e). \quad (14)$$

4. Results and discussion

Fig. 5 depicts the fit of the Eq. (8b) to AISA observations from 18 of March 2011. The fitting according to Eq. (9) is performed to median reflectances observed for nine canopy cover (C) classes (for eight classes when open areas are ignored). The class-stratified data are applied for the fitting procedure, since the random fluctuations in the observations at the processing resolution of 10 m are high. This causes instability to the used non-linear optimization procedure (search result dependent on the starting value), which is avoided by the use of averaged/median values. When the fitting is performed for the class-wise median values the effect of occasional very high reflectance values are better removed

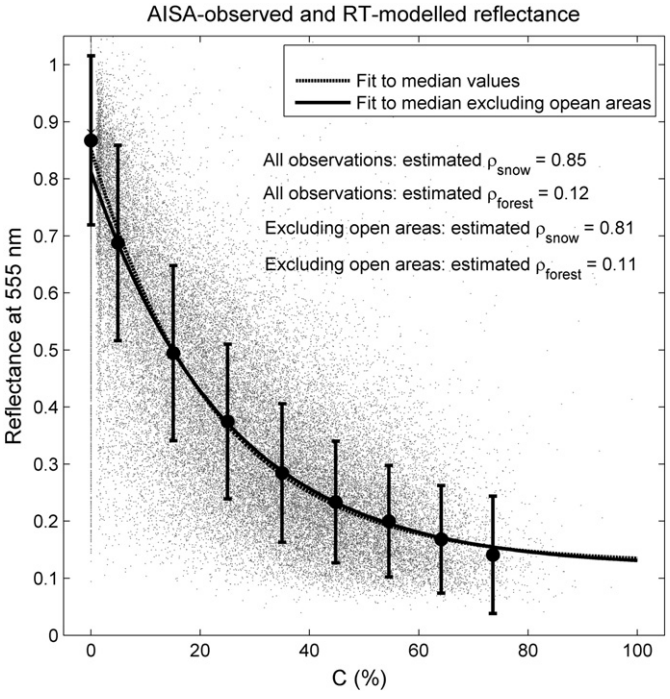

Fig. 5. Scene reflectance at 555 nm as a function of canopy cover (C). The scene reflectance model (Eq. 8b) is fitted to AISA observations of the Sodankylä site by optimizing the values of $\rho_{\lambda,forest}$, $\kappa_{e,forest}$ and $\rho_{\lambda,snow}$. Spatial resolution is 10 m. The fitting was done for C class stratified median values. Bars indicate ±standard deviation from the C class-wise mean values.

than when using mean values. Note that the actual individual data points are also shown in Fig. 5.

The effect of spatial scale to modeling is shown in Fig. 6. The dotted line shows the model prediction (Eq. 8b) when fitting parameters (ρ_{forest}, $\kappa_{e,forest}$ and ρ_{snow}) are estimated from data sets processed to a resolution of 10 m corresponding to Fig. 5. Solid line depicts the model prediction when the same parameters are estimated from data averaged to a resolution of 100 m with a two-dimensional box convolution function (10×10 window). The individual data points in 100 m resolution are presented by dots, and the standard deviations from class-wise averages are shown by solid bars, respectively. According to the results, model parameters slightly change as a function of spatial resolution, as the canopy cover (C) averaged to a scale of 100 m does not include values exceeding 59% (refer to Table 2) unlike in the scale of 10 m. However, the radiative transfer model according to Eq. (8b) well describes the behavior of reflectance. This implies that the suggested modeling approach is a valid methodology to describe the influence of forests for instruments with varying spatial resolution characteristics.

The comparison of radiative transfer (RT) approach Eq. (8b) with a linear mixing model (Eq. 10) indicates a higher validity for the RT than for the linear mixing model. The correlation coefficient between the reflectance predicted by Eq. (8b) is as high as $R^2 = 0.91$ for all data points processed to 100 m spatial resolution, whereas it is $R^2 = 0.87$ for the linear mixing formula; see Table 3 (the corresponding behavior of reflectance as a function of canopy cover is shown in Fig. 6). Table 3 presents the overall model fittings with respect to canopy cover (C), stem volume (V) and tree height (H), as well as the comparison of RT modeling performance with respect to linear mixing and polynomial fitting indicating the better performance of the RT approach, even though Eq. (10) applies two fitting parameters, whereas the radiative transfer model requires three parameters estimated by Eq. (9). Nevertheless, the results indicate that the behavior of reflectance is clearly non-linear and obeys well with Eq. (8b). If a second degree polynomial is fitted to data (three fitting parameters) we obtain about the same correlation coefficient ($R^2 = 0.918$) than with the exponential radiative transfer approach; see Table 3. However, the use of second degree polynomial lacks any physical significance, whereas both the RT approach and linear mixing model are based on physical assumptions.

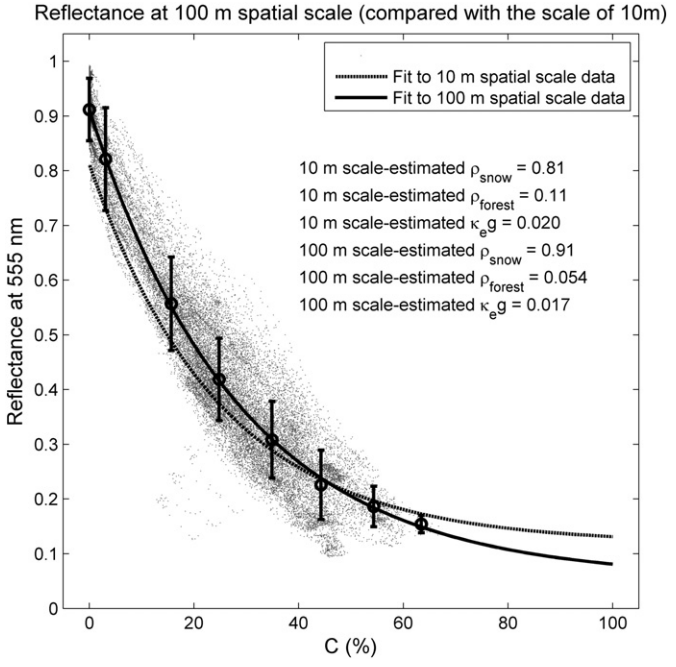

Fig. 6. Scene reflectance at 555 nm as a function of canopy cover for data averaged to spatial resolution of 100 m. The comparison for the model fitting at the scale of 10 m is also shown (dotted curve). Individual data points at the scale of 100 m are depicted by gray dots, whereas the error bars show the standard deviations from class stratified mean values. The case $C = 0\%$ is excluded in the fitting procedure (Eq. 9).

The effect of pixel (footprint) homogeneity to observed scene reflectance is investigated in Fig. 7. In practice, the AISA data is processed (block averaged) to a spatial grid of 100 m. Thereafter, each grid cell is assigned to represent either a homogenous or a heterogeneous target with respect to forest canopy cover (C) by analyzing the canopy cover at four sub-grid cells of each footprint of 100 m × 100 m. A footprint is considered as heterogeneous, if any of the four (50 m × 50 m-sized) sub-grid cells shows a value $C_{sub} < 0.5\ C_{ave}$ or $C_{sub} > 2 \cdot C_{ave}$, where C_{ave} stands for the canopy cover of the whole 100 m × 100 m pixel. Additionally, grid cell is considered as homogeneous, if all four sub-grid cells show a value $C_{sub} < 1\%$.

Both the data and model fittings by Eq. (9) in Fig. 7 indicate that the heterogeneity of forest cover within the pixel has an effect to the scene reflectance as a function of canopy cover fraction C. However, the results also show that the modeling approach of Eqs. (8a)–(8c) is appropriate even for forested targets heterogeneous at the scale of the applied instrument. This is also indicated by the two fit curves of Fig. 7. Additionally, Fig. 6 suggests that, if the mixture of homogeneous and heterogeneous pixels is corresponding to that of the Sodankylä site, the deviation of individual observations from the general fit curve is rather small.

As demonstrated by Fig. 7, the variability of forest canopy effects to scene reflectance is influenced by the structural heterogeneity of forest cover. On the other hand, results of earlier investigations, e.g. Niemi et al. (2012), suggest that variability of forest effects is related to the variability of bidirectional illumination conditions (which is the case with the applied AISA data). This is further shown in Fig. 8 that depicts the overall variability of forest scene reflectance due to varying illumination conditions (deep snow pack and snow-free pine canopy). The mast-borne spectrometer observations shown in Fig. 8 are obtained for 12 days during the year 2013 from 26 March to 12 April and for a single day in 2010 (18 March corresponding to airborne AISA data acquisition). Fig. 8 indicates the strong effect of bidirectional imaging conditions. For forward scattering cases the reflectance at 555 nm drops with increasing Sun zenith angle to values as low as about 0.07. For the backscatter, the behavior of reflectance is quite opposite; the reflectance shows high levels up to 0.17, and may even increase with the increasing Sun zenith angle. However, the standard deviation of reflectance corresponds well with the reflectance variability of mast-borne spectrometer observations carried out simultaneously with airborne AISA-imaging (Niemi et al., 2012).

Fig. 9 depicts the prediction of the variability of the two-way forest canopy transmissivity t^2 as a function of canopy cover (C) based on Eq. (14). The results of Fig. 9 are determined using the value $\mathrm{var}(\kappa_e) = 0.00083\%^{-1}$ for the variance of forest canopy extinction coefficient. This value is estimated by Eq. (13) using the following parameter values, mainly based on mast-borne spectrometer measurements carried out simultaneously with AISA imaging (green data points in Fig. 8):

- $\kappa_{e,forest} g'(\theta) = 0.017\%^{-1}$ (from Table 3)
- $C = 40\%$ (canopy cover fraction in the forest plot observed by the mast-borne spectrometer (Niemi et al., 2012))
- $\rho_{forest} = 0.089$ (Niemi et al., 2012)
- $\mathrm{var}(\rho_{forest}) = (0.01)^2$ (Niemi et al., 2012)
- $\rho_{snow} = 0.98$ (Salminen et al., 2009)
- $\mathrm{var}(\rho_{snow}) \approx 0$ (observations from a single day applied)
- $\mathrm{var}(R) = (0.03)^2$ (observed variance for the single day measurements according to Niemi et al. (2012)).

The results of Fig. 9 suggest that the relative standard deviation of the variability of forest canopy transmissivity is 13% (due to the variability of BRDF configuration). One should note that this variability is only a valid estimate for cases of near-nadir observations as the sensor look angle in mast-borne experiments is fixed to 11° off nadir. It should be

Table 3
Fitting parameters of the RT model for reflectance at 555 nm and comparison of its performance with that of the linear mixing model and second degree polynomial fitting curve. The spatial scale of modeling is 100 m.

Forest parameter	RT model fitting parameters			R^2 (coefficient of determination) for different modeling approaches		
	$\rho_{\lambda,forest}$,	$\kappa_{e,forest}g'(\theta)$[a]	$\rho_{\lambda,snow}$	Radiative transfer (RT)	Linear mixing[b]	2nd deg. polynomial[a]
Canopy cover, C (%)	0.054	0.017 (1/%)	0.91	0.920[c]	0.865	919
Stem volume, V (m^3/ha)	0.112	0.015 (ha/m^3)	0.86	0.878[d]	0.758	0.864
Tree height, H (m)	0.116	0.069 (1/m)	0.96	0.841[e]	0.750	0.843

[a] Note that $g'(\theta) \approx 1.96$.
[b] All individual data points in algorithm training and testing.
[c] Seven classes (excluding $C = 0\%$) in algorithm training, all individual points in testing.
[d] Eleven classes (excluding $V = 0$ m^3/ha) in algorithm training, all individual points in testing.
[e] Eight classes (excluding $H = 0$ m) in algorithm training, all individual points in testing.

noted that Fig. 9 considers the variability of forest scene reflectance for a single day, March 18, 2010, corresponding to airborne data acquisition (see green symbols in Fig. 8). In that case the range in azimuthal difference between the sensor and the Sun angles is from 31° to 107° (i.e. both forward and backscattering geometries are included as source of transmissivity variability in Fig. 9, but sensor look angle is constant).

5. Summary and conclusions

This investigation shows that the approach using the zeroth order solution of the radiative transfer (RT) equation to describe forest effects to scene reflectance is valid for typical boreal forests. The results also indicate that this applies both to homogeneous or heterogeneous forest scenes (satellite/remote sensing data footprints). However, the parameterization of the model changes according to heterogeneity of the sensor's footprint. The obtained results justify the appliance of apparent forest canopy transmissivity to describe the influence of forest to reflectance, as done in the *SCAmod* method for the continental scale FSC monitoring. The analyses carried out here are limited to the wavelength band of 545–565 nm as this range (MODIS band 4) is operationally feasible to snow monitoring purposes. Apart from that, Heinilä et al. (2014) presented results using several wavelengths for comparison.

The feasibility of the zeroth order RT approach is also compared with the use of linear mixing model of scene reflectance. This analysis shows that the non-linear RT approach describes the scene reflectance of a snow-covered boreal forest more realistically than the linear mixing model (in case when shadows on tree crowns and surface are not modeled separately, which is a relevant suggestion when considering the use of models for large scale snow mapping applications). The results also suggest that the consideration of forest canopy by estimating the apparent canopy transmissivity from the applied satellite data, as performed in *SCAmod* approach, is in practice a more feasible approach than the use of modeled value of forest canopy extinction coefficient. That is the case, since the modeled value of extinction coefficient is slightly dependent on scale, as indicated in Figs. 6 and 7. When the apparent canopy transmissivity is estimated from the employed satellite data, this effect is eliminated.

The obtained results also demonstrate the variability of scene reflectance due to varying illumination and bidirectional measurement geometries; see Fig. 8 for mast-borne observations. Also in the case of the applied airborne data set, the variability of reflectance around the curve of model prediction is in the same order, and apparently predominantly caused by these factors; see Figs. 6 and 7. However, the results show that the overall variability is quite small. This suggests that simple

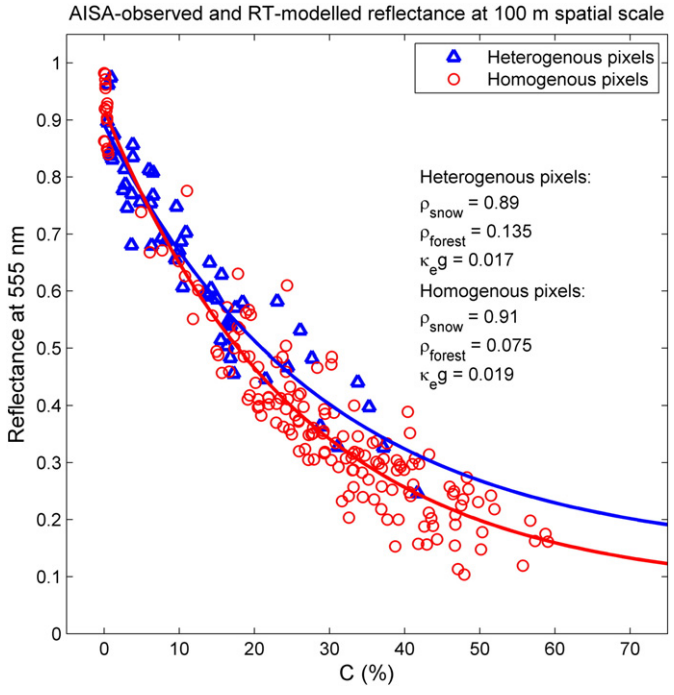

Fig. 7. Scene reflectance at 555 nm at the scale of 100 m separately for pixels homogenous or heterogeneous with respect to forest cover. Red and blue curves show the model fittings according to Eq. (9).

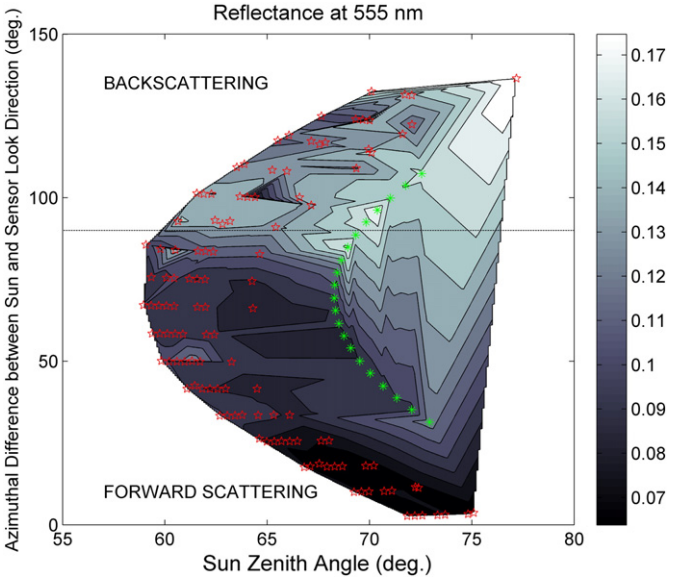

Fig. 8. Bidirectional reflectance of the forest plot of mast-borne spectrometer observations. Red and green symbols show the geometry of actual measurements representing full snow cover condition. The behavior of reflectance (contour plot) is interpolated from measurements at the locations of all the symbols (red pentagrams and green asterisks). Red pentagrams depict observations conducted for 12 days at different hours of day during the year 2013. Measurements from 18 March 2010 coinciding airborne data acquisition are shown by green asterisks.

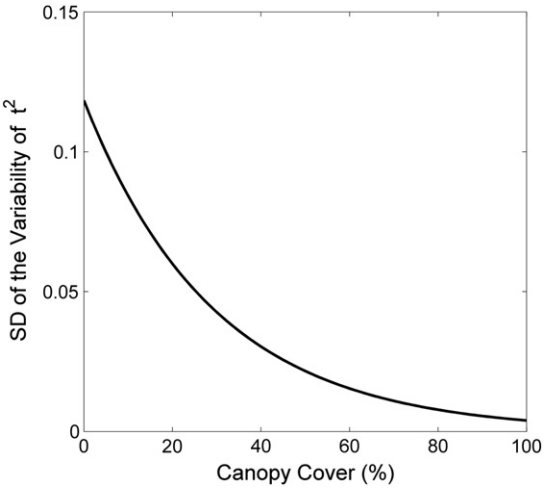

Fig. 9. Estimated variability of forest canopy transmissivity at 555 nm due to variability of illumination conditions for near-nadir observations.

RT approach is feasible to describe bulk extinction and reflectance (scattering) properties of forests on average.

Acknowledgments

The work has been supported by the national CLEEN (Cluster for Energy and Environment) MMEA (Measurement, Monitoring and Environmental Assessment) research program, funded by TEKES, and CLIMWATER (Climate Change and Water Cycle: Effect to Water Resources and their utilization in Finland) FICCA program project, funded by the Academy of Finland (Grant number 140915). This work has been also supported by the Airborne Imaging Spectroscopy Application and Research on Earth Sciences (AISARES) graduate school of the University of Helsinki.

References

Barnett, T. P., Adam, J. C., & Lettenmaier, D. P. (2005). Potential impacts of a warming climate on water availability in snow dominated regions. *Nature, 438*, 303–309.
Betts, A. K., & Ball, J. H. (1997). Albedo over the boreal forest. *Journal of Geophysical Research, 102*, 901–909.
Brown, R. D., & Mote, P. W. (2009). The response of northern hemisphere snow cover to a changing climate. *Journal of Climate, 22*, 2124–2145.
Choi, G., Robinson, D. A., & Kang, S. (2010). Changing northern hemisphere snow seasons. *Journal of Climate, 23*, 5305–5310.
Dietz, J. A., Kuenzer, C., Gessner, U., & Dech, S. (2012). Remote sensing of snow — A review of available methods. *International Journal of Remote Sensing, 33*, 4094–4134.
Dietz, J., Wohner, C., & Kuenzer, C. (2012). European snow cover characteristics between 2000 and 2011 derived from improved MODIS daily snow cover products. *Remote Sensing, 4*, 2434–2454.
Dozier, J., Green, R., Nolin, A., & Painter, T. (2009). Interpretation of snow properties from imaging spectrometry. *Remote Sensing of Environment, 113*, S25–S37.
Frei, A., Tedesco, M., Lee, S., Foster, J., Hall, D. K., Kelly, R., & Robinson, D. A. (2012). A review of global satellite-derived snow products. *Advances in Space Research, 50*, 1007–1029.
Hall, D. K., Foster, J. L., Salomonson, V. V., Klein, A. G., & Chien, J. Y. L. (2001). Development of a technique to assess snow-cover mapping errors from space. *IEEE Transactions on Geoscience and Remote Sensing, 39*, 432–438.
Hall, D. K., Foster, J. L., Verbyla, D. L., Klein, A. G., & Benson, C. S. (1998). Assessment of snow-cover mapping accuracy in a variety of vegetation-cover densities in central Alaska. *Remote Sensing of Environment, 66*, 129–137.
Hall, D. K., & Riggs, G. A. (2007). Accuracy assessment of the MODIS snow products. *Hydrological Processes, 21*, 1534–1547.
Hall, D. K., Riggs, G. A., Salomonson, V. V., DiGirolamo, N. E., & Bayr, K. J. (2002). MODIS snow-cover products. *Remote Sensing of Environment, 83*, 181–194.
Heinilä, K., Salminen, M., Pulliainen, J., Cohen, J., Metsämäki, S., & Pellikka, P. (2014). The effect of boreal forest canopy to reflectance of snow covered terrain based on airborne imaging spectrometer observations. *International Journal of Applied Earth Observation and Geoinformation, 27*, 31–41.
Helfrich, S. R., McNamara, D., Ramsay, B. H., Baldwin, T., & Kasheta, T. (2007). Enhancements to, and forthcoming developments in the interactive multisensory snow and ice mapping system (IMS). *Hydrological Processes, 21*, 1576–1586.
Klein, A. G., & Barnett, A.C. (2003). Validation of daily MODIS snow cover maps of the upper Rio Grande River Basin for the 2000–2001 snow year. *Remote Sensing of Environment, 86*, 162–176.
Klein, A. G., Hall, D. K., & Riggs, G. A. (1998). Improving snow cover mapping in forests through the use of a canopy reflectance model. *Hydrological Processes, 12*, 1723–1744.
Li, X., & Strahler, A. H. (1985). Geometric-optical modeling of a conifer forest canopy. *IEEE Transactions on Geoscience and Remote Sensing, 23*, 705–721.
Li, X., Strahler, A. H., & Woodcock, C. E. (1995). A hybrid geometric optical-radiative transfer approach for modeling albedo and directional reflectance of discontinuous canopies. *IEEE Transactions on Geoscience and Remote Sensing, 33*, 467–480.
Liu, J., Woodcock, C., Melloh, R., Davis, R., McKenzie, C., & Painter, T. (2008). Modeling the view angle dependence of gap fractions in forest canopies: Implications for mapping fractional snow cover using optical remote sensing. *Journal of Hydrometeorology, 9*, 1005–1019.
Luojus, K., Pulliainen, J., Rott, H., Nagler, T., Solberg, R., Wiesmann, A., Derksen, C., Metsämäki, S., Malnes, El, & Bojkov, B. (2010). ESA DUE GlobSnow — Global snow data-base for climate research. *Proceedings of the ESA Living Planet Symposium, June 28–July 2, 2010, Bergen, Norway, SP-686*.
METLA (2010). *Finnish statistical yearbook of forestry*. Vammala, Finland: Finnish Forest Research Institute, 62.
Metsämäki, S., Anttila, S., Huttunen, M., & Vepsäläinen, J. (2005). A feasible method for fractional snow cover mapping in boreal zone based on a reflectance model. *Remote Sensing of Environment, 95*, 77–95.
Metsämäki, S., Mattila, O. -P., Pulliainen, J., Niemi, K., Luojus, K., & Böttcher, K. (2012). An optical reflectance model-based method for fractional snow cover mapping applicable to continental scale. *Remote Sensing of Environment, 123*, 508–521.
Metsämäki, S., Vepsäläinen, J., Pulliainen, J., & Sucksdorff, Y. (2002). Improved linear interpolation method for the estimation of snow-covered area from optical data. *Remote Sensing of Environment, 82*, 64–78.
Niemi, K., Metsämäki, S., Pulliainen, J., Suokanerva, H., Böttcher, K., Leppäranta, M., & Pellikka, P. (2012). The behaviour of mast-borne spectra in a snow-covered boreal forest. *Remote Sensing of Environment, 124*, 551–563.
Nolin, A. W. (2004). Towards retrieval of forest cover density over snow from the multi-angle imaging spectroradiometer (MISR). *Hydrological Processes, 18*, 3623–3636.
Nolin, A. W. (2010). Recent advances in remote sensing of seasonal snow. *Journal of Glaciology, 56*, 1141–1150.
Painter, T. H., Dozier, J., Roberts, D. A., Davis, R. E., & Green, R. O. (2003). Retrieval of subpixel snow-covered area and grain size from imaging spectrometer data. *Remote Sensing of Environment, 85*, 64–77.
Painter, T. H., Rittger, K., McKenzie, C., Slaughter, P., Davis, R. E., & Dozier, J. (2009). Retrieval of subpixel snow covered area, grain size, and albedo from MODIS. *Remote Sensing of Environment, 113*, 868–879.
Parajka, J., & Blöschl (2006). Validation of MODIS snow cover images over Austria. *Hydrology and Earth System Sciences, 10*, 679–689.
Pulliainen, J., Heiska, K., Hyyppä, J., & Hallikainen, M. (1994). Backscattering properties of boreal forests at the C- and X-bands. *IEEE Transactions on Geoscience and Remote Sensing, 32*, 1041–1050.
Ramsay, B. H. (1998). The interactive multisensory snow and ice mapping system. *Hydrological Processes, 12*, 1537–1546.
Rittger, K., Painter, T. H., & Dozier, J. (2013). Assessment of methods for mapping snow cover from MODIS. *Advances in Water Resources, 51*, 367–380.
Robinson, D. A., Dewey, K. F., & Heim, R. R., Jr. (1993). Global snow cover monitoring: An update. *Bulletin of the American Meteorological Society, 74*, 1689–1696.
Rosema, A., Verhoef, W., Noorbergen, H., & Borgesius, J. J. (1992). A new forest light interaction model in support of forest monitoring. *Remote Sensing of Environment, 42*, 23–41.
Salminen, M., Pulliainen, J., Metsämäki, S., Kontu, A., & Suokanerva, H. (2009). The behaviour of snow and snow-free surface reflectance in boreal forests: Implications to the performance of snow covered area monitoring. *Remote Sensing of Environment, 113*, 907–918.
Salomonson, V. V., & Appel, I. (2004). Estimating fractional snow cover from MODIS using the normalized difference snow index. *Remote Sensing of Environment, 89*, 351–360.
Salomonson, V. V., & Appel, I. (2006). Development of the Aqua MODIS NDSI fractional snow cover algorithm and validation results. *IEEE Transactions on Geoscience and Remote Sensing, 44*, 1747–1756.
Schlerf, M., & Atzberger, C. (2006). Inversion of a forest reflectance model to estimate structural canopy variables from hyperspectral remote sensing data. *Remote Sensing of Environment, 100*, 281–294.
Tomppo, E., Haakana, M., Katila, M., & Peräsaari, J. (2008). *Multi-source national forest inventory — Methods and applications. (Managing forest ecosystems)*. New York: Springer.
Vaughan, D.G., Comiso, J. C., Allison, I., Carrasco, J., Kaser, G., Kwok, R., Mote, P., Murray, T., Paul, F., Ren, J., Rignot, E., Solomina, O., Steffen, K., & Zhang, T. (2013). Observations: Cryosphere. In T. F. Stocker, D. Qin, G. -K. Plattner, M. Tignor, S. K. Allen, J. Boschung, A. Nauels, Y. Xia, V. Bex, & P.M. Midgley (Eds.), *Climate change 2013: The physical science basis. Contribution of working group I to the fifth assessment report of the intergovernmental panel on climate change* (pp. 317–382). Cambridge, United Kingdom and New York, NY, USA: Cambridge University Press.
Vikhamar, D., & Sohlberg, R. (2002). Subpixel mapping of snow cover in forests by optical remote sensing. *Remote Sensing of Environment, 84*, 69–82.
Vikhamar, D., & Solberg, R. (2003). Snow-cover mapping in forests by constrained linear spectral unmixing of MODIS data. *Remote Sensing of Environment, 88*, 309–323.